Available online at www.sciencedirect.com
ScienceDirect
Polymer 48 (2007) 5268–5278
polymer
www.elsevier.com/locate/polymer

Metallo-homopolymer and metallo-copolymers containing light-emitting poly(fluorene/ethynylene/(terpyridyl)zinc(II)) backbones and 1,3,4-oxadiazole (OXD) pendants

Yi-Yu Chen, Hong-Cheu Lin*

Department of Materials Science and Engineering, National Chiao Tung University, Hsinchu, Taiwan ROC

Received 8 May 2007; received in revised form 15 June 2007; accepted 19 June 2007
Available online 23 June 2007

Abstract

A series of novel metallo-polymers containing light-emitting poly(fluorene/ethynylene/(terpyridyl)zinc(II)) backbones and electron-transporting 1,3,4-oxadiazole (OXD) pendants (attached to the C-9 position of fluorene by long alkyl spacers) were synthesized by self-assembled reactions. The integrated ratios of ^{1}H NMR spectra reveal a facile result to distinguish the well-defined main-chain metallo-polymeric structures which were constructed by different monomer ligand systems (i.e. single, double, and triple monomer ligands with various pendants). Furthermore, UV–vis and photoluminescence (PL) spectral titration experiments were carried out to verify the metallo-polymeric structures by varying the molar ratios of zinc(II) ions to monomers. As a result, the enhancement of thermal stability (T_d) and quantum yields were introduced by the metallo-polymerization, and their physical properties were mainly affected by the nature of the pendants. The photophysical properties of these metallo-polymers exhibited blue PL emissions (around 418 nm) with quantum yields of 34–53% (in DMF). In contrast to metallo-polymers containing alkyl pendants, the quantum yields were greatly enhanced by introducing 1,3,4-OXD pendants but reduced by carbazole (CAZ) pendants. Moreover, electroluminescent (EL) devices with these light-emitting metallo-polymers as emitters showed green EL emissions (around 550 nm) with turn-on voltages of 6.0–6.5 V, maximum efficiencies of 1.05–1.35 cd A^{-1} (at 100 mA/cm^{-2}), and maximum luminances of 2313–3550 cd/m^2 (around 15 V), respectively.

Keywords: Metallo-polymers; 1,3,4-Oxadiazole; Carbazole

1. Introduction

Recently, the use of transition or rare earth metal complexes to build up polymeric light-emitting diode (PLED) devices has attracted much attention because of the enhancement in EL efficiency [1–5]. Chan and co-workers demonstrated that the construction of conjugated polymers made of ruthenium bipyridyl complexes can enhance the light-emitting performance by utilizing energy transfer from the triplet excited state [6–8]. A whole set of coordination polymers consisting of ditopic electro- and photo-active terpyridyl ligands complexed with zinc ions were recently published by Che and co-workers [9]. These coordination polymers exhibit different emission wavelengths ranging from violet to yellow colors with high PL quantum yields, and these polymers were successfully applied to PLED devices. Hence, tuning electroluminescent (EL) properties could be achieved through the incorporation of different transition metal complexes into polymer main chains [6–14]. Moreover, it is confirmed that due to the d^{10} zinc(II) species the phenomena of intraligand charge transfers (ILCTs) happen between terpyridine/zinc(II) complexes and chromophores even in fully conjugated metallo-polymers [9–12]. Therefore, the incorporation of terpyridine/zinc(II) moieties into metallo-polymers with fine-tuned chromophores can provide good quantum yields

* Corresponding author. Tel.: +886 3 5712121x55305; fax: +886 3 5724727.
E-mail address: linhc@mail.nctu.edu.tw (H.-C. Lin).

0032-3861/$ - see front matter © 2007 Elsevier Ltd. All rights reserved.
doi:10.1016/j.polymer.2007.06.040

and thermal stabilities, and thus to have the potential to become high-performance emissive or host materials in PLED applications [15–17].

However, some important and fundamental challenges remain to solve, including the maximization of luminescence and power efficiency, the designs and syntheses of new materials for purer colors, and the modes of addressing devices for full-color displays with optimized resolutions. A major factor responsible for poor device performance is that the charge injection and transportation in emissive materials are generally unbalanced. This imbalance arises because the energy barrier between the indium tin oxide (ITO) anode and the highest occupied molecular orbital (HOMO) level of an emissive material is different from that between the metal cathode and its lowest unoccupied molecular orbital (LUMO) level [18]. In previous studies, molecular and polymeric 1,3,4-oxadiazole (OXD) derivatives are one of the most widely studied classes of electron injection and/or hole-blocking materials, mainly because of their electron deficiencies, high photoluminescence quantum yields, and chemical stabilities [18–22]. Therefore, the introduction of electron-deficient OXD groups into the C-9 position of the fluorene units increase the electron affinities of resulting polymers and lead to more balanced charge injection and transporting properties as well as better recombination behavior [23–25].

In this context, various electron- and hole-transporting substituents, i.e. 1,3,4-oxadiazole (OXD) and carbazole (CAZ) pendants, were incorporated into poly(fluorene/ethynylene/(terpyridyl)zinc(II))-based metallo-copolymers (as shown in Scheme 1). In addition, the ^{1}H NMR, thermal, photophysical, and electrochemical properties were investigated as well. Furthermore, the PLED applications of metallo-copolymers as emitters in multilayer EL devices with two different heterojunction configurations of ITO/PEDOT:PSS/polymer/TPBI[2,2′,2″-(1,3,5-benzenetriyl)tris[1-phenyl-1*H*-benzimidazole]/LiF/Al and ITO/PEDOT:PSS/polymer/BCP(2,9-dimethyl-4,7-diphenyl-1,10-phenanthroline)/ALQ(tris(8-hydroxyquinoline)-aluminium)/LiF/Al were studied.

2. Experimental

2.1. Measurements

^{1}H NMR spectra were recorded on a Varian Unity 300 MHz spectrometer using $CDCl_3$ and DMSO-d_6 solvents. Elemental analyses were performed on a HERAEUS CHN-OS RAPID elemental analyzer. Phase transition temperatures were determined by differential scanning calorimetry (DSC, model: Perkin Elmer Diamond) with a heating and cooling rate of 10 °C/min. Thermogravimetric analysis (TGA) was conducted on a Du Pont Thermal Analyst 2100 system with a TGA 2950 thermogravimetric analyzer at a heating rate of 10 °C/min under nitrogen. Melting points were determined by a Buchi SMP-20 capillary melting point apparatus. Viscosity measurements were proceeded by 10% weight of polymer solutions (in NMP) in contrast to those proceeded by the same condition of monomer solutions (with viscosity $\eta = 6$ cP) on a BROOKFILEL DV-III+RHEOMETER system (100 rpm, spindle number: 4) at 25 °C. UV–visible (UV–vis) absorption spectra were recorded in dilute DMF solutions (10^{-5} M) on a HP G1103A spectrophotometer, and fluorescence spectra were obtained on a Hitachi F-4500 spectrophotometer. Fluorescence quantum yields were determined by comparing the integrated photoluminescence (PL) intensity of coumarin-1 in ethanol with a known quantum yield (ca. 5×10^{-6} M, quantum yield = 0.73). Cyclic voltammetry (CV) was performed at a scanning rate of 100 mV/s on a BAS 100 B/W electrochemical analyzer, which was equipped with a three-electrode cell. Pt wire was used as a counter electrode, and an Ag/AgCl electrode was used as a reference in the CV measurements. The CV experiments were performed by solid samples immersed into electrochemical cell containing 0.1 M tetrabutylammonium hexafluorophosphate (Bu_4NPF_6) solutions (in DMF) with a scanning rate of 100 mV/s at room temperature under nitrogen. UV–vis and PL titrations were performed by the 1.0×10^{-5} M of monomer solutions in the solvent of $CH_3CN/CHCl_3$ (2/8 in vol.) were titrated with 50 μl aliquots of 3.9×10^{-4} M of $Zn(OAc)_2$ solutions in the same solvent composition as described. The addition was done stepwise and the formation of Zn(II)-coordination polymers was monitored by UV–vis spectroscopy. Polymer thin solid films in UV–vis and PL measurements were prepared by spin-coating polymers on quartz substrates from DMF solutions with a concentration of 10 mg/ml. A series of EL devices with two device configurations of ITO/PEDOT:PSS/polymer/TPBI-(2,2′,2″-(1,3,5-benzenetriyl)tris[1-phenyl-1*H*-benzimidazole])//LiF/Al and ITO/PEDOT:PSS/polymer/BCP(2,9-dimethyl-4,7-diphenyl-1,10-phenanthroline)/AlQ(tris(8-hydroxyquinoline)-aluminium)/LiF/Al were made, where TPBI and AlQ were used as electron-transporting layers, and BCP was used as a hole-blocking layer collocated to AlQ. ITO substrates were routinely cleaned by ultrasonic treatments in detergent solutions and diluted water, followed by rinsing with acetone and then with ethanol. After drying, ITO substrates were kept in oxygen plasma for 4 min before being loaded into the vacuum chamber. The solutions (10 mg/ml) of light-emitting materials in DMF were spin-coated on glass slides precoated with indium tin oxide (ITO) having a sheet resistance of ~20 Ω/square and an effective individual device area of 3.14 mm^2. The spin coating rate was 6000 rpm for 60 s with PEDOT:PPS, 4000 rpm for 60 s with resulting polymers, and the thicknesses of PEDOT:PPS and polymers were measured with an Alfa Step 500 Surface Profiler (Tencor). TPBI, BCP, and AlQ were thermally deposited at a rate of 1–2 Å/s under a pressure of $\sim 2 \times 10^{-5}$ Torr in an Ulvac Cryogenic deposition system. Under the same deposition conditions and systems, one layer of LiF was thermally deposited as a cathode at a rate of 0.1–0.2 Å/s, which was followed by capping with aluminum.

2.2. Materials

Chemicals and solvents were reagent grades and purchased from Aldrich, ACROS, TCI, and Lancaster Chemical Co. Solvents were purified and dried according to standard

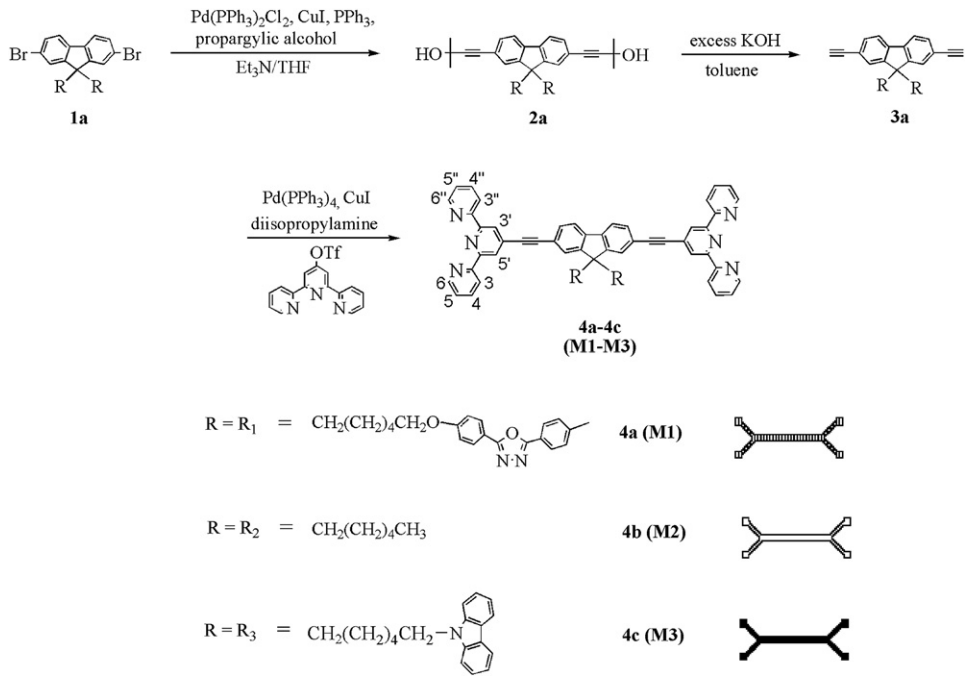

Scheme 1. Synthetic routes of monomers **4a–4c** (**M1–M3**).

procedures. Chromatography was performed with Merck silica gel (mesh 70–230) and basic aluminum oxide, which was deactivated with 4 wt% of water. 4′-[[(Trifuroromethyl)sulfonyl]oxy]-2,2′:6′,6″-terpyridines and compounds **1a**, **4b** (**M2**), and **4c** (**M3**) were prepared and purified according to literature procedures [11,12,25–27]. The synthetic routes of monomers **4a–4c** (**M1–M3**) and metallo-polymers **P1–P4** are illustrated in Schemes 1 and 2.

2.3. Synthetic procedures of monomers

2.3.1. Compound *2a*

To a solution of compoumd (**1a**) (28 mmol) in 60 mL of THF/Et_3N (1/1), 3-methyl-1-butyn-3-ol (84 mmol) was added. After the solution was degassed with nitrogen for 30 min, $Pd(PPh_3)_2Cl_2$ (0.28 mol), PPh_3 (11 mol), and CuI (2.8 mmol) were added. The reaction was then refluxed at 70 °C under N_2 for 12 h. The solvent was removed under reduced pressure. The resulting solid was extracted with CH_2Cl_2/H_2O then dried over $MgSO_4$. The crude product was purified by column chromatography (silica gel, hexane/ethyl acetate = 4/1) to afford a white solid; mp 76–77 °C. ^{1}H NMR (300 MHz, $CDCl_3$): δ 8.01–8.05 (m, 8H), 7.60 (d, $J = 7.8$ Hz, 2H), 7.39–7.42 (m, 4H), 7.32 (d, $J = 8.4$ Hz, 4H), 6.94 (d, $J = 9$ Hz, 4H), 3.90 (t, $J = 6.3$ Hz, 4H), 2.44 (s, 6H), 2.04 (s, 2H), 1.95 (br, 4H), 1.59–1.66 (m, 16H), 1.13–1.18 (m, 12H). Yield: 77%. FABMS: *m/e* 996; $C_{65}H_{66}N_4O_6$ requires *m/e* 998.50.

2.3.2. Compound *3a*

A mixture of **2a** (1.63 mmol) and KOH (6.5 mmol) in 60 mL of 2-propanol was heated to reflux under N_2 with a vigorous stirring for 3 h. The solvent was then removed and crude product was purified by column chromatography (silica gel, hexane) to afford a white solid; mp 82–83 °C. ^{1}H NMR (300 MHz, $CDCl_3$): δ 7.99–8.04 (m, 8H), 7.64 (d, $J = 7.8$ Hz, 2H), 7.47–7.50 (m, 4H), 7.32 (d, $J = 8.4$ Hz, 4H), 6.95 (d, $J = 9$ Hz, 4H), 3.91 (t, $J = 6.3$ Hz, 4H), 3.16 (s, 2H), 2.44 (s, 6H), 1.97 (br, 4H), 1.59–1.66 (m, 4H), 1.13–1.20 (m, 12H). Yield: 77%. FABMS: *m/e* 882; $C_{59}H_{54}N_4O_4$ requires *m/e* 882.41.

2.3.3. Monomer *4a (M1)*

Compound **3a** (0.5 mmol) and 4′-[[(trifuroromethyl)sulfonyl]oxy]-2,2′:6′,6″-terpyidine (1.1 mmol) were dissolved in nitrogen-degassed benzene, then $[Pd^0(PPh_3)_4]$ (70 mg, 0.06 mmol) was added followed by the addition of 20 ml of nitrogen-degassed ^{i}Pr$_2$NH. The solution was then heated to 70 °C. After complete consumption of starting materials, the solvent was evaporated and the product was purified by column chromatography (alumina, hexane/dichloromethane = 10/1 in vol.) to afford a white solid; mp 115–116 °C. ^{1}H NMR (300 MHz, $CDCl_3$): δ 8.7 (d, $J = 5.1$ Hz, 4H), 8.60–8.64 (m, 8H), 7.93–7.97 (m, 8H), 7.86 (t, $J = 7.8$ Hz, 4H), 7.75 (d, $J = 8.7$ Hz, 2H), 7.58–7.61 (m, 4H), 7.33–7.37 (m, 4H), 7.30 (d, $J = 8.1$ Hz, 4H), 6.93 (d, $J = 8.7$ Hz, 4H), 3.92 (t, $J = 6.6$ Hz, 4H), 2.43(s, 6H), 2.08 (br, 4H), 1.64 (br, 4H), 1.22 (br, 12H). Yield: 75%. FABMS: *m/e* 1343; $C_{89}H_{72}N_{10}O_4$ requires *m/e* 1344.57. Anal. Calcd for $C_{89}H_{72}N_{10}O_4$: C, 79.44; H, 5.39; N, 10.42; O, 4.76. Found: C, 80.15; H, 5.77; N, 10.22; O, 4.41.

2.4. Synthetic procedures of metallo-polymers

2.4.1. Metallo-homopolymer *P1*

To monomer **4a** (**M1**) (0.52 mmol) in 30 ml of NMP solution, zinc acetate (0.52 mmol) in NMP (10 ml) was added

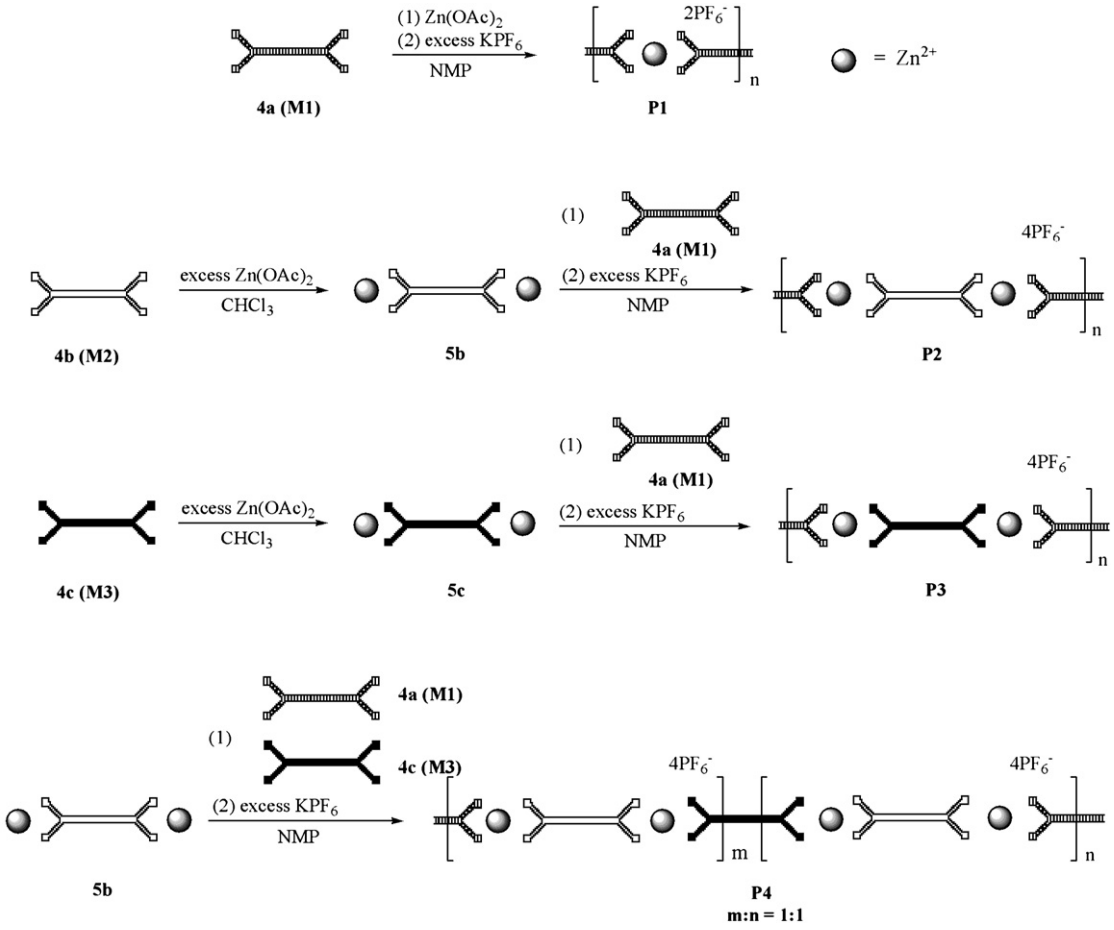

Scheme 2. Synthetic routes of metallo-polymers **P1**–**P4**.

dropwise. The resulting solution was heated at 105 °C under nitrogen atmosphere. After stirring for 24 h, excess KPF_6 (1.2 mmol) was added into the hot solution. The resulting solution was poured into methanol and the precipitate obtained was purified by repeated precipitations using NMP and ether. The polymers were dried under vacuum at 60 °C for 24 h and collected as yellow solids. Yields: 78–82%.

2.4.2. Metallo-alt-copolymer *P2*

To zinc acetate (1.25 mmol) in 20 ml of NMP (*N*-methyl-pyrrolidinone) solution, monomer **4b** (**M2**) (0.61 mmol) in NMP (20 ml) was added dropwise. After stirring at r.t. for 2 h, monomer **4a** (**M1**) (0.64 mmol) was also added dropwise. The resulting solution was heated at 105 °C under a nitrogen atmosphere. After stirring for 24 h, excess KPF_6 (2.6 mmol) was added into the hot solution. The resulting solution was poured into methanol and the precipitate obtained was purified by repeated precipitations using NMP and ether. The polymers were dried under vacuum at 80 °C for 24 h and collected as yellow solids. Yields: 74–80%.

2.4.3. Metallo-alt-copolymer *P3*

The procedure is analogous to that described for **P2**. Yield: 80–84%.

2.4.4. Metallo-copolymer *P4*

To zinc acetate (0.92 mmol) in 20 ml of NMP (*N*-methyl-pyrrolidinone) solution, monomer **4b** (**M2**) (0.45 mmol) in NMP (20 ml) was added dropwise. After stirring at r.t. for 2 h, mixture monomers **4a** (**M1**) and **4c** (**M3**) (0.42 mmol, **4a** (**M1**):**4c** (**M3**) = 1:1) was also added dropwise. The resulting solution was heated at 105 °C under nitrogen atmosphere. After stirring for 24 h, excess KPF_6 was added into the hot solution. The resulting solution was poured into methanol and the precipitate obtained was purified by repeated precipitations using NMP and ether. The polymer was dried under vacuum at 80 °C for 24 h and collected as a yellow solid. Yield: 80%.

3. Results and discussion

3.1. Synthesis and characterization

The synthetic routes of monomers **4a**, metallo-homopolymer **P1** and metallo-copolymers **P2**–**P4** are illustrated in Schemes 1 and 2. Metallo-homopolymer **P1** was obtained by refluxing monomer **4a** (**M1**) with $Zn(OAc)_2$ at a ratio of 1:1 in NMP solution and followed by subsequent anion exchange [11,12]. The key steps in the syntheses of metallo-*alt*-copolymers were first to functionalize two end terpyridyl units of

monomers **4b** (**M2**) and **4c** (**M3**) with $Zn(OAc)_2$ at a ratio of 1:2 to afford complexes **5b** and **5c**, respectively. Then, complexes **5b** and **5c** as initiators were coordinated with monomer **4a** (**M1**) (see Scheme 2) at a ratio of 1:1 (as a sequential-coupling method), respectively, to obtain metallo-*alt*-copolymers **P2** and **P3** [11]. Moreover, metallo-copolymer **P4** was obtained by reacting the mixture of monomers **4a** (**M1**) and **4c** (**M3**) (at a ratio of 1:1) with complex **5b** (monomer mixture:complex **5b** = 1:1). In contrast to other polymerization methods, i.e. the Witting or Heck coupling reactions, there are three points worthy to be noted. First, the reactive lability of zinc(II) ions and the stability of six-coordinate bis-terpyridine zinc(II) moieties allow self-assembled reactions to take place under refluxing conditions [3–5,9]. Second, the present procedure does not need any catalysts. Third, the chemical structures of metallo-copolymers can be controlled by proper stoichiometries of metals and monomers [11,12].

3.2. Structural characterization with ^1H NMR

^1H NMR spectra of monomers **4a–4c** (**M1–M3**), complexes **5b** and **5c** and metallo-polymers **P1–P4** were recorded in DMSO-d_6 as shown in Fig. 1. Compared with ^1H peaks of monomers **4b** (**M2**) and **4c** (**M3**) in our previous study [11], those in terpyridyl units of complexes **5b** and **5c** show the same downfield shift effect in proton peaks of (6,6″)-, (5,5″)-, (4,4″)-, (3′,5′)-, and (3,3″)-H. Furthermore, proton peaks of (4,4″)-H in terpyridyl units of complexes **5b** and **5c** overlap with ^1H peaks of fluorene units. It appears that the formation of complexes **5b** and **5c** can be, respectively, proven by the disappearance of original ^1H peaks in terpyridyl units of monomers **4a** and **4b** (**M1 and M2**) in the mixture of zinc ions and monomers at a ratio of 2:1 [11]. The formation of homopolymer **P1** is clearly indicated by the appearance of a new set of ^1H peaks and the absence of the original ^1H peaks in terpyridyl units, which belong to the uncomplexed monomer **4a** (**M1**). (The assignments of ^1H peaks of the terpyridyl units for all polymers are made by asterisks with respect to 4-chloro-terpyridine Zn^{2+} complexes). In terms of ^1H peaks of 1,3,4-OXD and carbazole (CAZ) pendants, there are no obvious changes in chemical shifts among monomers **4a** (**M1**), **4c** (**M3**) and polymers **P3**, **P4**. Therefore, the most up-shifted ^1H peaks in the terpyridyl units of polymers **P3** and **P4** could be overlapped with the ^1H peaks of these pendants. To distinguish the structural differences among these main-chain metallo-polymers **P1–P4**, it is feasible to compare the relative integrated ratios of the ^1H peaks. As a result, the integrated ratios of the ^1H peaks in the terpyridyl units (*A for **P1**, *A1 for **P2**, *A2 for **P3**, and *A3 for **P4**) and the ^1H peaks of the alkyl chains (spacer $-CH_2-$) attached to 1,3,4-OXD (**B** for **P1**, **B1** for **P2**, **B2** for **P3**, and **B3** for **P4**) and CAZ units (**C2** for **P3** and **C3** for **P4**) of these polymers are compared. It reveals that the relative integrated ratios are *A/B = 0.5, *A1/B1 = 1, *A2/B2 = 1, and *A3/B3 = 2 for metallo-polymers **P1**, **P2**, **P3**, and **P4**, respectively, which suggests that the integrated ratios of polymers were consistent with the monomer amounts containing pendant 1,3,4-OXD units [11].

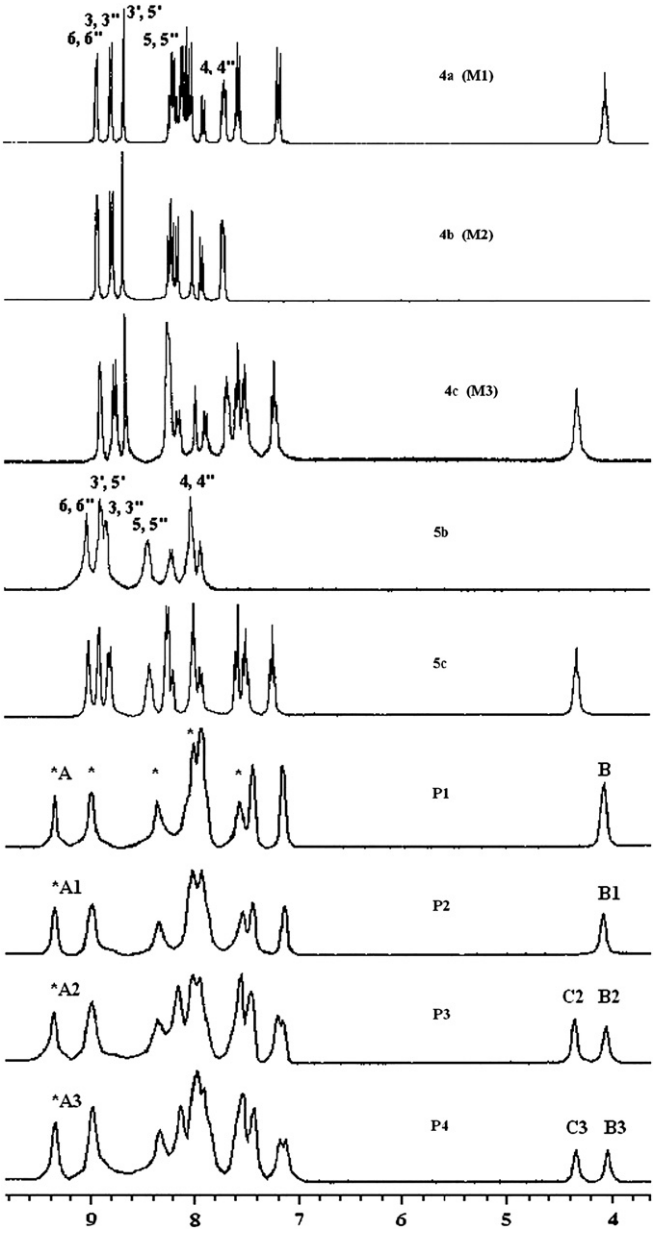

Fig. 1. ^1H NMR spectra of monomers **4a–4c** (**M1–M3**), complexes **5a** and **5b**, and metallo-polymers **P1–P4** in DMSO-d_6.

In contrast to the relative integrated ratio of **B2/C2** (=1.1) in polymer **P3**, that of **B3/C3** was 1 for polymer **P4**. According to these results, the input ratios (molecular ratios) of monomers for polymerization were very similar to the output ratios (the relative integrated ratios of ^1H NMR) of the metallo-polymers. Consequently, the amounts of monomer ligands incorporated in the monomer ligand-based metallo-polymers can be confirmed by ^1H NMR [28–30].

3.3. Thermal and viscosity properties

The thermal and viscosity properties of monomers **4a–4c** (**M1–M3**) and metallo-polymers **P1–P4** were studied by thermogravimetric analysis (TGA) and rheometry as summarized in Table 1. The decomposition temperatures (T_d) (5%

Table 1
Physical properties of metallo-polymers **P1**–**P4**

Polymer	T_d (°C)[a]	η (cP)[b,c]	$E^{red/peak}$ (V)[d]	E^{LUMO} (eV)[e]	E^{HOMO} (eV)[f]	Band gap (eV)[g]
P1	355	11	−1.54 (r)	−3.10	−6.26	3.16
P2	389	10	−1.54 (r)	−3.04	−6.20	3.16
P3	366	10	−1.54 (r)	−2.88	−6.03	3.15
P4	356	9	−1.55 (r)	−2.87	−6.02	3.15

[a] The decomposition temperatures (T_d) (5% weight loss) were determined by TGA with heating rates of 20 °C/min^{-1} under N_2 atmosphere. The T_d values were 221 °C for **4a** (**M1**), 351 °C for **4b** (**M2**), and 354 °C for **4c** (**M3**), respectively.
[b] The viscosities of metallo-polymers (10% in weight) in NMP solutions at 25 °C (100 rpm, spindle number: 4) were determined by rheometer system.
[c] Solutions of monomers **4a**–**4c** (**M1**–**M3**) (10% in weight) in NMP (with viscosities $\eta = 6$–7 cP, 25 °C) were used as references to determine the viscosities of metallo-polymers.
[d] Reduction peaks in N_2-purged DMF, r in parentheses means reversible.
[e] LUMO energy levels were calculated from the measured reduction potentials versus the ferrocene/ferrocenium couple in DMF solutions.
[f] HOMO energy levels were estimated from the measured optical band gaps and LUMO energy levels.
[g] Optical band gaps were estimated from the absorption spectra in solutions by extrapolating the tails of the lower energy peaks.

weight loss measured by TGA) of monomers under nitrogen atmosphere were ranged from 221 to 351 °C, and those of polymers were ranged from 355 to 389 °C. In contrast to monomers, polymers exhibited slightly enhanced thermal stability due to the increased rigidity of the main-chain structures [8]. As the bulky OXD and CAZ pendants are attached to the backbones of the metallo-polymers, it leads to reduced rigidity of the polymers [31,32]. Hence, compared with polymers **P1**, **P3**, and **P4** containing more bulky OXD and CAZ pendants, **P2** shows the highest T_d value among these metallo-polymers due to its higher molar ratio of less bulky alkyl pendants. This behavior was also confirmed by that the T_d value (422 °C) of metallo-homopolymer containing **M2** (with alkyl pendants) is larger than that (399 °C) of metallo-homopolymer containing **M3** (with CAZ pendants) in our previous report, [11] and both T_d values are larger than that (355 °C as shown in Table 1) of metallo-homopolymer **P1** containing **M1** (with OXD pendants). Moreover, the same trend of the pendant size effect on the T_g values were also observed in the monomers, i.e., **4b** (**M2** with alkyl pendant) = 103 °C > **4c** (**M3** with CAZ pendant) = 92 °C > **4a** (**M1** with OXD pendant) = 67 °C, so molecular structures with larger pendant groups have lower T_g values. This obviously indicates that the presence of OXD and CAZ pendants in these metallo-polymers suppresses the crystallinity (and chain aggregation) of the polymers effectively. Similar results were also observed in poly(fluorene)-based copolymers containing various 1,3,4-oxadiazole dendritic pendants [25]. However, all metallo-polymers **P1**–**P4** did not show any phase transition temperatures, including T_g. It suggested that the fully aromatic conjugated main-chain structures may induce the aggregation in metallo-polymers **P1**–**P4** by π–π stacking and thus to reduce the phase transition behavior [11]. In conclusion, the thermal properties were truly affected by the nature of different pendants incorporated into the polymers.

To further confirm the structures of metallo-polymers, molecular weights of these metallo-polymers should be investigated. However, these polymers showed poor solubilities in THF, CH_3Cl, and alcoholic solvents, so standard measurements of molecular weights by GPC (gel permeation chromatography) could not be proceeded. Therefore, the relative viscosities of polymers to monomers were carried out to support the formation of polymeric structures. Solutions of monomers **4a**, **4b** (**M1**, **M2**) (10% weight ratio) in NMP with viscosities $\eta = 6$–7 cP at 25 °C were used as references to determine the viscosities of the respective polymers. In comparison with the viscosities of monomers **4a**–**4c** (**M1**–**M3**), those of metallo-polymers **P1**–**P4** exhibit increased viscosities ($\eta =$ 9–11 cP) by adding Zn^{2+} ions, and the ratios of relatively increased viscosities of polymers to those of monomers were in the range of 1.50–1.66. Similar phenomena were also reported in our previous study [11].

3.4. Electrochemical properties

The electrochemical behavior of polymers were studied by cyclic voltammetry (CV), and the electrochemical properties are summarized in Table 1. The lowest unoccupied molecular orbital (LUMO) energy levels were estimated from reduction potentials by the reference energy level of ferrocene (4.8 eV below the vacuum level) according to the following equation: $E^{LUMO} = [-(E^{onset} - 0.45) - 4.8]$ eV [26,27]. However, the oxidation potentials of all metallo-polymers were not detectable, so the highest occupied molecular orbital (HOMO) energy levels can be estimated by the sums of LUMO energy levels and optical band gaps. All metallo-polymers exhibit reversible reduction peaks around −1.54 V in cathodic scans (up to −2.5 V). These peaks are attributed to the reduction of terpyridyl-based moieties [9,11]. The absence of oxidation peaks in the anodic scans (up to 1 V) of these polymers, are due to the metal oxidation of d^{10} zinc(II) ion species being extremely difficult to be observed [33–35]. The optical band gaps were estimated from absorption spectra in DMF solutions by extrapolating the tails of the lowest energy peaks, and the optical band gaps of these polymers were ranged from 3.15 to 3.16 eV. Since metallo-polymers **P1**–**P4** possess similar backbone structures, there are no obvious differences in the optical band gaps. The electrochemical results indicate that the incorporation of 1,3,4-OXD pendant groups into the backbones of metallo-polymers will efficiently reduce the LUMO energy levels, and thus to reduce the electron injection barrier between the cathode and the emitters [36,37].

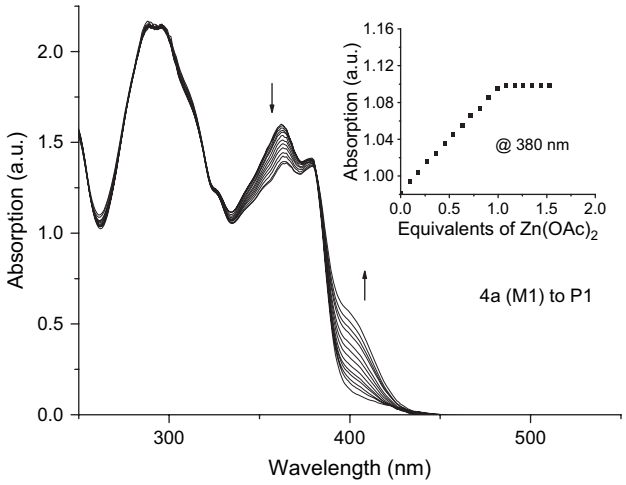

Fig. 2. UV–vis spectra acquired in the process of **4a** (**M1**) to **P1** upon the titration of monomer **4a** (**M1**) in $CH_3CN/CHCl_3$ (2/8 in vol.) with $Zn(OAc)_2$. The spectra are shown at selected ranges of Zn^{+2}:**4a** (**M1**) = 0–1. The inset shows the normalized absorption at 380 nm as a function of Zn^{+2}:**4a** (**M1**) ratio.

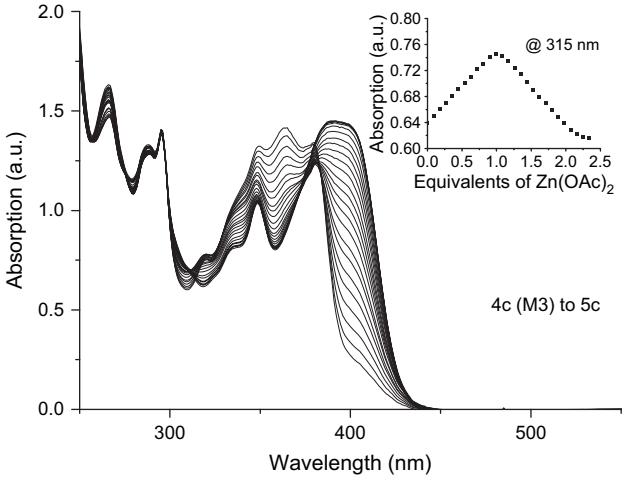

Fig. 4. UV–vis spectra acquired (in the process of **4c** (**M3**) to **5c**) upon the titration of monomer **4c** (**M3**) in $CH_3CN/CHCl_3$ (2/8 in vol.) with $Zn(OAc)_2$. The spectra are shown at selected ranges of Zn^{+2}:**4c** (**M3**) = 0–2. The inset shows the normalized absorption at 315 nm as a function of Zn^{+2}:**4c** (**M3**) ratio.

3.5. UV–vis and photoluminescence titration

To characterize the formation of metallo-hompolymer **P1** and complexes **5a** and **5b**, the UV–visible (UV–vis) and photoluminescence (PL) titration experiments are clear ways to investigate their stepwise changes. Fig. 2 described that upon addition of Zn^{2+} ions to monomer **4a** (**M1**) reaching a ratio of Zn^{+2}:**4a** (**M1**) = 1:1, the spectra revealed clear shifts of three absorption bands at 364, 379, and 405 nm along with one isosbestic point, which suggests that an equilibrium occurred between a finite number of spectrorscopically distinct species. The titration curve (in the inset of Fig. 3) showed a linear increase and a sharp end point at a ratio of Zn^{+2}:**4a** (**M1**) = 1:1, indicating the formation of metallo-homopolymer **P1**. The syntheses and characterization of metallo-homopolymers by adding Zn^{2+} ions to monomers **4b** (**M2**) or **4c** (**M3**) to the ratio of Zn^{+2}:**4b** (**M2**) = 1:1 or Zn^{+2}:**4c** (**M3**) = 1:1 have also been investigated [11]. Beyond this point (Figs. 3 and 4), the subsequent addition of Zn^{2+} ions induced new peaks at 279, 285, 348, and 394 nm for complex **5b** (332, 348, and 393 nm for **5c**) as well as new isosbestic points to form, which points out that an equilibration arose between spectroscopically distinct species. Thus, Figs. 5 and 6 depicted that the ratios of Zn^{2+} ions to monomers **4b** (**M2**) or **4c** (**M3**) are above 1:1, and the depolymerization is driven by the formation of chain-terminating complexes **5b** or **5c** [11,38]. All of the UV–vis titration spectra showed the lowest absorption around λ_{abs} = 394–404 nm, which corresponds to a charge transfer occurring between the electron-rich central fluorenyl

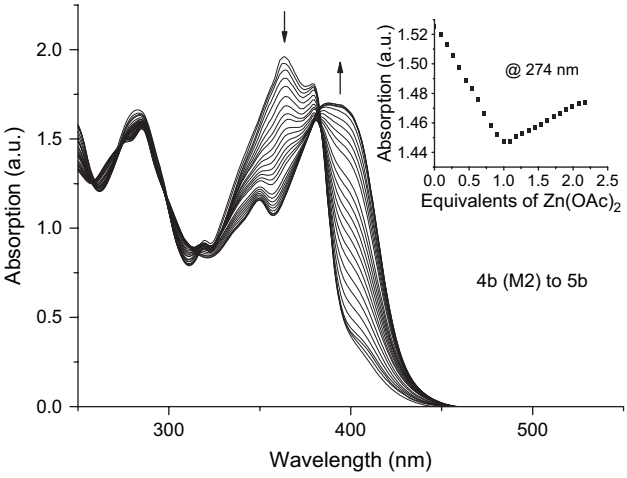

Fig. 3. UV–vis spectra acquired (in the process of **4b** (**M2**) to **5b**) upon the titration of monomer **4b** (**M2**) in $CH_3CN/CHCl_3$ (2/8 in vol.) with $Zn(OAc)_2$. The spectra are shown at selected ranges of Zn^{+2}:**4b** (**M2**) = 0–2. The inset shows the normalized absorption at 274 nm as a function of Zn^{+2}:**4b** (**M2**) ratio.

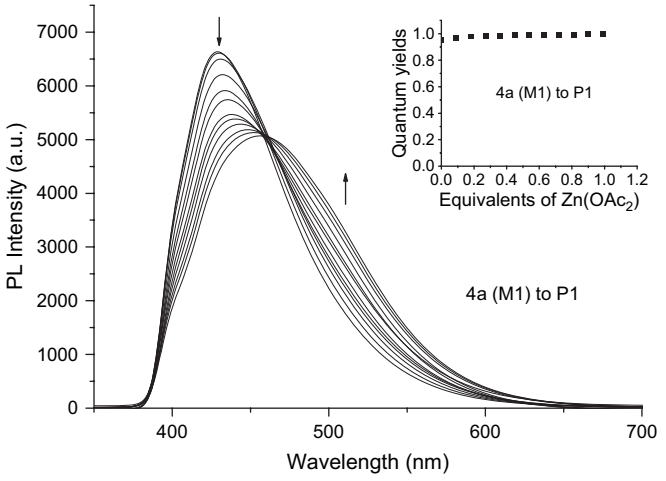

Fig. 5. PL spectra acquired upon the titration of monomer **4a** (**M1**) in $CH_3CN/CHCl_3$ (2/8 in vol.) with $Zn(OAc)_2$. The spectra are shown at selected ranges of Zn^{+2}:**4a** (**M1**) = 0–1. The inset shows the quantum yields as a function of Zn^{+2}:**4a** (**M1**) ratio.

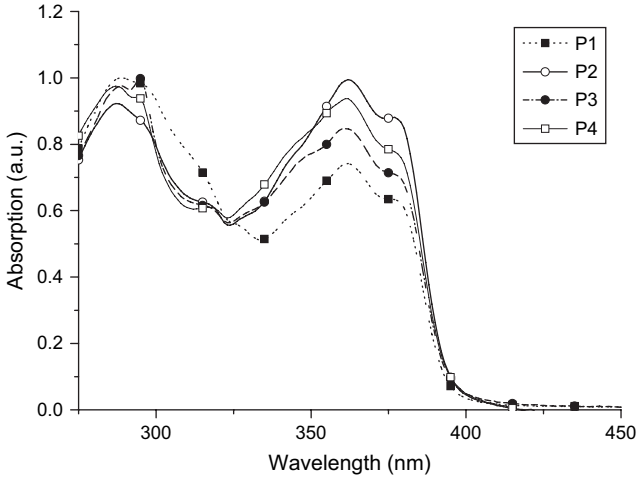

Fig. 6. Normalized UV–vis spectra of metallo-polymers **P1**–**P4** in DMF solutions.

components and the electron-deficient metal-coordinated terpyridyl moieties [38,39]. In Fig. 5, monomer **4a** (**M1**) showed an emission band around 429 nm. As the ratio of Zn^{2+}:**4a** (**M1**) reached 1:1, a new emission band at 456 nm was induced. The PL quantum yields of medium complexes, i.e. the ratio of Zn^{+2}:**4a** (**M1**) gradually approached 1:1 in the inset of Fig. 5, scarcely increased followed by increasing molar ratio of Zn^{+2} ions. Therefore, the PL quantum yields of metallo-homopolymer **P1** can be marginally enhanced by attaching 1,3,4-OXD pendant groups to the polymer backbones. Furthermore, the monomer **4b** (**M2**) exhibited a similar PL result by the formation of metallo-homopolymer reaching the ratio of Zn^{2+}:**4b** (**M2**) = 1:1, except for the metallo-homopolymer synthesized from monomer **4c** (**M3**) with CAZ pendants possessing a much lower quantum yield (in solution) than its monomer **4c** [11]. In titration experiments, not only different complexed situations could be confirmed by various stoichiometries, but also the alteration of photophysical properties between the monomers and polymers were also observed during the coordination processes.

3.6. Photophysical properties

The photophysical measurements of monomers **4a**–**4c** (**M1**–**M3**) and metallo-polymers **P1**–**P4** were carried out by UV–vis absorption and photoluminescence (PL) experiments in both dilute DMF (*N*,*N*-dimethylformamide) solutions (with some solubility problems) and solid films, and their photophysical properties are presented in Table 2. In Fig. 6, similar absorption features of polymers **P1**–**P4** were observed at 286, 320, and 377 nm. In general, other absorption peaks can be assigned to pendant groups (i.e. $\lambda_{abs} = 295$ and 300 nm for CAZ and OXD pendants, respectively) and these absorption peaks attributed to pendant groups also can assist to confirm the metallo-copolymer structures. PL emissions of all monomers and polymers are assigned to intraligand (π^*–π) fluorescence. They showed purple-blue emission colors in DMF solutions, where the values of PL emission peaks ($\lambda_{max,PL}$) were around 414 nm (in DMF) with quantum yields (Φ) of 20–33% for monomers **4a**–**4c** (**M1**–**M3**) and $\lambda_{max,PL} \sim 417$ nm (in DMF) with quantum yields (Φ) of 34–53% for metallo-polymers **P1**–**P4**. The enhancement of the quantum yields in metallo-polymer was attributed to the polymerization procedure and similar results were reported in literature [9,11,12]. Nevertheless, PL emissions from the OXD pendants were not observed, even when metallo-polymers were excited at the absorption peaks of the OXD pendants. This indicates the existence of efficient energy transfer from the OXD pendants to the polymer backbones [26]. Comparing PL quantum yields of metallo-copolymers **P2**–**P4** with the same molar ratio (50%) of OXD pendants, the order of PL quantum yields (in solutions) is **P2** > **P4** > **P3**, which is reverse to the order of the molar ratio of CAZ pendants in metallo-polymers **P2**–**P4**, i.e. **P2** (0% CAZ) < **P4** (25% CAZ) < **P3** (50% CAZ). It suggests that of the metallo-polymers containing **M2** (with alkyl pendants) have larger PL quantum yields than those containing **M3** (with CAZ pendants). This behavior fits well with the PL quantum yield (53%) of metallo-homopolymer **P1** containing **M1** (with OXD pendants) being larger than that (23%) [11] of metallo-homopolymer containing **M2** (with alkyl pendants), and also larger than that (11%) [11] of metallo-homopolymer containing **M3** (with CAZ pendants). Overall, in contrast to metallo-polymers containing alkyl pendants, the quantum yields were greatly enhanced by introducing 1,3,4-OXD pendants but reduced by carbazole (CAZ) pendants. Hence, PL quantum yields of metallo-polymers were truly affected by incorporating different monomer ligands into main-chain polymeric structures.

Table 2
Photophysical properties of monomers **4a**–**4c** (**M1**–**M3**) and metallo-polymers **P1**–**P4**

Compound	$\lambda_{abs,\ sol}$ (nm)[a]	$\lambda_{max,\ PL,\ sol}/\Phi_{PL,\ sol}$ (nm)[a,b,c]	$\lambda_{abs,\ film}$ (nm)	$\lambda_{max,\ PL,\ film}$ (nm)
4a (**M1**)	292, 363, 378	414/0.33	–	–
4b (**M2**)	285, 319, 363, 373	415/0.20	–	–
4c (**M3**)	287, 294, 319, 347, 364, 374	414/0.25	–	–
P1	288, 327, 361, 377	418/0.53	289, 298, 337, 399	500
P2	287, 317, 361, 378	416/0.51	299, 354, 413	502
P3	287, 294, 318, 361, 377	416/0.34	289, 354, 408	502 (472, 533)
P4	288, 295, 316, 348, 361, 378	416/0.35 (401)	297, 353, 410	500 (473)

[a] Concentration of 1×10^{-6} M in DMF.
[b] Coumarin-1 in ethanol (ca. 5×10^{-6} M, quantum yield = 0.73) used as a reference to determine the quantum yields of PL in solutions.
[c] The PL emission shoulders are shown in the parentheses.

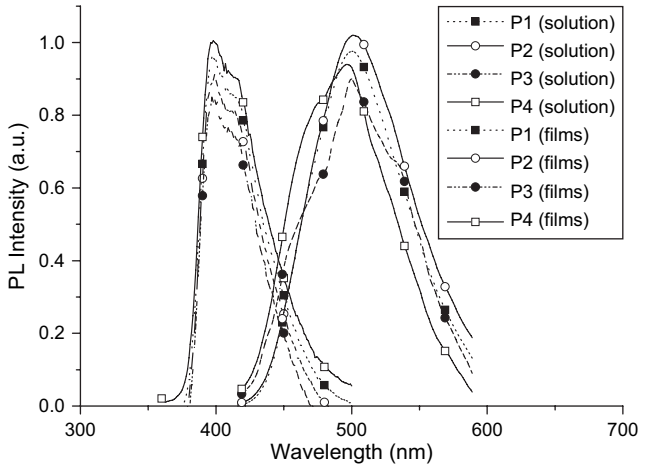

Fig. 7. Normalized PL spectra of metallo-polymers **P1**–**P4** in solutions and solid films.

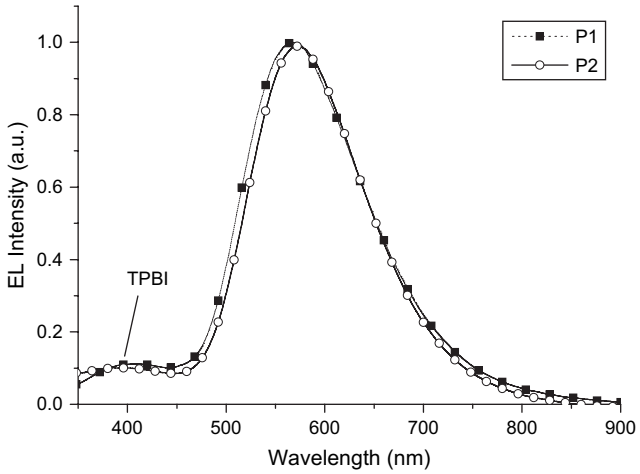

Fig. 8. Normalized EL spectra of PLED devices with configurations of ITO/PEDOT:PSS/polymer (**P1**–**P2**)/TPBI/LiF/Al at 10 V.

Regarding solid films of these metallo-polymers, they emitted blue to green colors with PL values of $\lambda_{max,PL}$ in the range 509–520 nm (Fig. 7). According to PL emissions of polymer films, all polymers showed large Stokes shifts (ca. 83–104 nm) in contrast to their PL emissions in solutions, which were attributed to the excimer formation resulting from π–π stacking of aromatic interaction in solid films [40,41]. When the bulky pedants (i.e. CAZ) were attached to the C-9 position of fluorene units, they were able to suppress the excimer formation as shown in our previous result [9]. However, metallo-copolymers **P3** and **P4** only showed small shoulders around 472 nm (see Fig. 7), which correspond to the emissions of polymer backbones, and metallo-polymers **P1** and **P2** even with dominant excimer emissions around 500 nm. Nevertheless, compared with our previous result of metallo-homopolymers containing CAZ pendants, OXD pendants in all metallo-polymers **P1**–**P4** did not suppress the excimer formation efficiently, which might be due to more flexible pendant configurations (with lower T_g values) of metallo-polymers containing 1,3,4-OXD pendants in comparison with those containing CAZ pedants.

3.7. Electroluminescence (EL) properties

Two device configurations were applied in the EL measurements, where the metallo-polymers were used as an emission layer and PEDOT:PSS was utilized as a hole-transporting layer. Either TPBI or BCP/ALQ was used as an electron-transporting layer, and the results are separately discussed as follows:

(a) ITO/PEDOT:PSS/polymer(**P1**–**P2**)/TPBI/LiF/Al devices. Good photoluminescence properties exhibited by solutions of metallo-polymers **P1** and **P2** suggest both polymers are suitable candidates for fabrication of PLED devices, and devices with configurations of ITO/PEDOT:PSS (40–55 nm)/polymer(**P1**–**P2**) (50–65 nm)/TPBI (40 nm)/LiF (1 nm)/Al (150 nm) were fabricated. Fig. 8 shows normalized EL spectra of metallo-polymers **P1** and **P2**, and an emission band around 570 nm and a small shoulder around 400 nm originated from TPBI emissions were observed [42,43]. It is worthy of noting that the EL spectra of PLED devices do not resemble their corresponding PL spectra in solid films (as shown in Fig. 7). This is presumably due to the EL and PL emissions originating from different excited states and/or ground states [11,44]. In comparison with the HOMO values of polymers **P1** (−6.26 eV) and **P2** (−6.20 eV), TPBI (−6.20 eV) layer could not block holes from emitters sufficiently for polymers **P1** and **P2** in the PLED devices [42,43], so they exhibited very similar results to each other. Hence, no further investigation has been done in the other TBPI-based PLED devices regarding polymers **P3** and **P4**.

(b) ITO/PEDOT:PSS/polymer/BCP/ALQ/LiF/Al devices. Green EL emissions were obtained for all metallo-polymers with configurations of ITO/PEDOT:PSS (40–55 nm)/polymer(**P1**–**P4**) (50–65 nm)/BCP (10 nm)/ALQ (30 nm)/LiF (1 nm)/Al (150 nm), and the electroluminescence properties are listed in Table 3. Fig. 9 illustrates the normalization EL spectra of metallo-polymers **P1**–**P4** with emission bands around 550 nm. Similarly, the EL spectra of BCP/ALQ devices do not resemble their corresponding PL spectra in solid films due to the same reason as explained in the TPBI-based PLED devices. At a bias voltage of 10 V, all PLED devices in Fig. 9 show green emissions with $\lambda_{max,\ EL}$ values around 550 nm and their EL intensities were enhanced by increasing the bias voltages. The turn-on voltages of all PLED devices based on BCP/ALQ were approximately 6.0–6.5 V. The power efficiency and maximum luminance of PLED devices for all polymers were ranged from 1.05 to 1.35 cd A^{-1} (at 100 mA/cm^{-2}) and 2313–3550 cd/m^2 (at 14–15 V), respectively. The current density–voltage (I–V) and luminance–voltage (L–V) characteristic curves of PLED devices containing metallo-polymers **P1**–**P4** are shown in Figs. 10 and 11, and similar turn-on voltages for both current density and luminance demonstrate that a matched balance of both injection and transportation

Table 3
Electroluminescence (EL) properties of PLED devices[a] containing a layer of emitting metallo-polymers **P1**–**P4**

Polymer	$\lambda_{max,\ EL}$ (nm)	V_{on} (V)[b]	Max. luminescence (cd/m^2) (V)	Power efficiency (cd A^{-1})[c]	CIE coordinates (x and y)
P1	549	6.5	2913 (14.5)	1.12	(0.41, 0.52)
P2	549	6.5	3550 (15)	1.35	(0.41, 0.52)
P3	551	6.0	3320 (15)	1.25	(0.41, 0.55)
P4	550	6.5	2313 (14.5)	1.05	(0.41, 0.52)

[a] Device structure: ITO/PEDOT:PSS/polymer(**P1**–**P4**)/BCP/AlQ/LiF/Al, where the metallo-polymer (**P1**–**P4**) is an emitting layer.
[b] V_{on} is the turn-on voltage.
[c] Power efficiencies were obtained at 100 mA/cm^2.

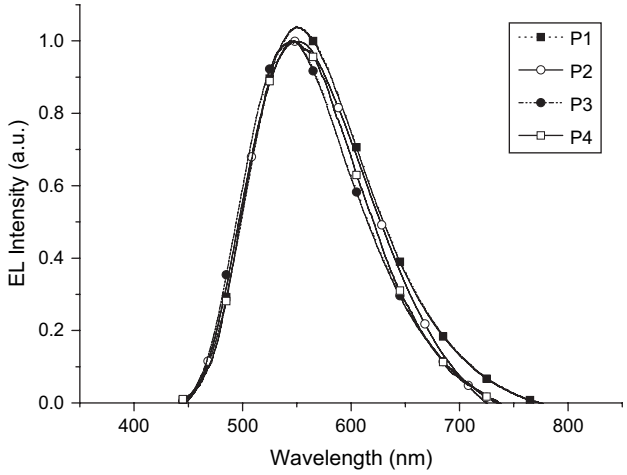

Fig. 9. Normalized EL spectra of PLED devices with configurations of ITO/PEDOT:PSS/polymer (**P1**–**P4**)/BCP/ALQ/LiF/Al at 10 V.

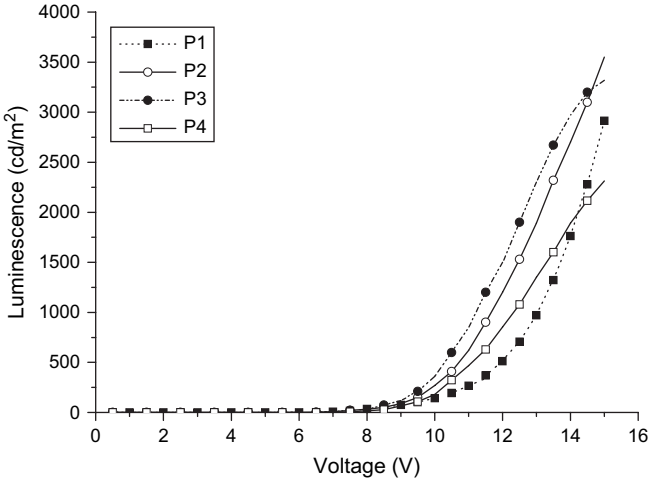

Fig. 11. Luminance–voltage (L–V) curves of PLED devices with configurations of ITO/PEDOT:PSS/polymer (**P1**–**P4**)/BCP/ALQ/LiF/Al.

in charges were achieved [26], which were much improved in contrast to TPBI-based PLED devices. The BCP layer (HOMO = −6.70 eV, LUMO = −3.20 eV) can offer a large hole barrier between BCP and the emitter but shows no influence on electron-transporting behavior of ALQ (HOMO = −6.00 eV, LUMO = −3.30 eV) [45]. As shown in Fig. 11, it indicates that no ALQ emission band was observed. The EL spectra of BCP/ALQ-based devices (polymers **P1** and **P2**) revealed less Stocke shifts (ca. 20 nm) than those of TPBI-based devices. The different timing for the charge arriving at the emitter region may be related to different electron mobilities for these two transporting materials [43,45,46]. From this result, it can be concluded that the incorporation of electron-transporting (OXD) or hole-transporting (CAZ) pendants into polymer backbones can improve the EL performance of the PLED devices [47].

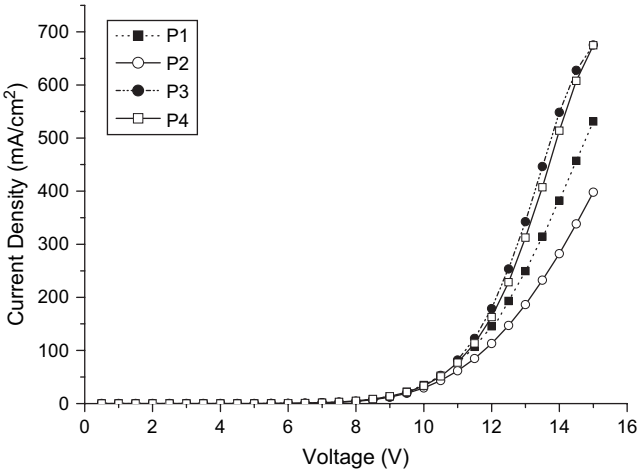

Fig. 10. Current density–voltage (I–V) curves of PLED devices with configurations of ITO/PEDOT:PSS/polymer (**P1**–**P4**)/BCP/ALQ/LiF/Al.

4. Conclusions

In summary, a series of novel poly(fluorene/ethynylene/(terpyridyl)zinc(II))-based metallo-polymers containing 1,3,4-OXD pedants were obtained by different stoichiometric ratios of complexes. Furthermore, the thermal, photophysical, and electroluminescence properties are greatly affected by the nature of the pendant groups in the C-9 position of fluorene via long alkyl spacers. The incorporation of various pendants into polymer backbones will change the rigidities and the thermal stability (as well as the T_d and T_g values) of the metallo-polymers. In comparison with metallo-polymers containing alkyl pendants, the quantum yields were greatly enhanced by introducing 1,3,4-OXD pendants but reduced by carbazole (CAZ) pendants. The enhancement of PL quantum yields by the introduction of 1,3,4-OXD pendants into metallo-polymers is due to the energy transfer happened between pedants and polymer backbones. By utilization of these metallo-polymers

as emitting materials to fabricate PLED devices, green EL emissions and high EL performance can be obtained in the double-heterojunction device structures with PEDOT as the hole-transporting material and either TPBI or BCP/ALQ as the electron-transporting material.

Acknowledgements

We thank the financial support from Chung-Shan Institute of Science and Technology (in Taiwan) and the National Science Council of Taiwan (ROC) through NSC 94-2113-M-009-005, and the instrumental support provided by Prof. Yu-Tai Tao (vacuum deposition) at Institute of Chemistry, Academia Sinica and Prof. Ching-Fong Shu (CV measurements) at Dept. of Applied Chemistry, National Chiao Tung Univ. (in Taiwan).

References

[1] Baldo MA, O'brien DF, Thompson ME, Forrest SR. Phys Rev B 1999; 60:14422.
[2] Lu W, Mi BX, Chan MCW, Hui Z, Zhu NY, Lee ST, et al. Chem Commun 2002;206.
[3] Andres PR, Schubert US. Adv Mater 2004;16:1043.
[4] Homeier H, Schubert US. Chem Soc Rev 2004;33:373.
[5] Schubert US, Eschbaumer C. Angew Chem Int Ed 2002;41:2892.
[6] Yu SC, Gong X, Chan WK. Macromolecules 1998;31:5639.
[7] Yu SC, Hou S, Chan WK. Macromolecules 1999;32:5251.
[8] Yu SC, Hou S, Chan WK. Macromolecules 2000;33:3259.
[9] Yu SC, Kwok CC, Chan WK, Che CM. Adv Mater 2003;15:1643.
[10] Dobrwa R, Würthner FJ. J Polym Sci Part A Polym Chem 2005;43:4981.
[11] Chen YY, Tao YY, Lin HC. Macromolecules 2006;39:8559.
[12] Chen YY, Lin HC. J Polym Sci Part A Polym Chem 2007;45:3243.
[13] Vogel V, Gohy JF, Lohmeijer BGG, Broek JAVD, Haase W, Schubert US, et al. J Polym Sci Part A Polym Chem 2003;41:3159.
[14] Holder E, Marin V, Alexeev A, Schubert US. J Polym Sci Part A Polym Chem 2005;43:2765.
[15] Chu Q, Pang Y. J Polym Sci Part A Polym Chem 2006;44:2338.
[16] Shunmugam R, Tew GN. J Polym Sci Part A Polym Chem 2005;43:5831.
[17] Tzanetos NP, Andreopoulou AK, Kallitsis JK. J Polym Sci Part A Polym Chem 2005;43:4838.
[18] Wang CS, Jung GY, Hua Y, Pearson C, Bryce MR, Petty MC, et al. Chem Mater 2001;13:1167.
[19] Kraft A, Grimsdale AC, Holmes AB. Angew Chem Int Ed Engl 1998;37: 402.
[20] Segura JL. Acta Polym 1998;49:319.
[21] Thelakkat M, Schmidt HW. Polym Adv Technol 1998;9:429.
[22] Mitschke U, Bauerle PJ. Mater Chem 2000;10:1471.
[23] Wu FI, Reddy S, Shu C, Liu MS, Jen AKY. Chem Mater 2003;15:269.
[24] Shu CF, Dodda R, Wu FI, Liu MS, Jen AKY. Macromolecules 2003;36: 6698.
[25] Wu CW, Lin HC. Macromolecules 2006;39:4298.
[26] Sung HH, Lin HC. J Polym Sci Part A Polym Chem 2005;43:2700.
[27] Sung HH, Lin HC. Macromolecules 2004;37:7945.
[28] Dobrwa R, Würthner F. Chem Commun 2002;1878.
[29] Dobrwa R, Lysetaka M, Ballester P, Grüne M, Würthner F. Macromolecules 2005;38:1315.
[30] Schmelz O, Rehahn M. e-Polymers 2002;47.
[31] Knapton D, Iyer PK, Rowan SJ, Weder C. Macromolecules 2006;31: 5639.
[32] Huang F, Wu H, Wang D, Wang W, Cao Y. Chem Mater 2004;16:708.
[33] Loiseau F, Pietro CD, Serroni S, Campagna S, Licciardello A, Manfredi A, et al. Inorg Chem 2001;40:4901.
[34] Hwang SH, Wang P, Moorefield CN, Godinez LA, Manriquez J, Bustos E, et al. Chem Commun 2005;4672.
[35] Lia G, Bhosaleb S, Taoa S, Guoa R, Bhosaleb S, Lia F, et al. Polymer 2005;46:5299.
[36] Xia C, Adviacula RC. Chem Mater 2001;13:1682.
[37] Jin Y, Kim JY, Park SH, Kim J, Lee S, Lee K, et al. Polymer 2005;46: 12158.
[38] Iyer PK, Beck JB, Weder C, Rowan SJ. Chem Commun 2005;319.
[39] Wang XY, Guerzo AD, Schmehl RH. Chem Commun 2002;2344.
[40] Desiraju GR, Gavezotti A. J Chem Soc Chem Commun 1989;621.
[41] Alcock NW, Barker PR, Haider JM, Hannon MJ, Painting CL, Pikramenou Z, et al. J Chem Soc Dalton Trans 2000;1447.
[42] Tao YT, Chuen CH, Ko CW, Peng JW. Chem Mater 2004;14:4256.
[43] Tao YT, Balasubramaniam E, Danel A, Tomasik P. Appl Phys Lett 2000; 77:933.
[44] Kwok CC, Yu SC, Sham ST, Che CM. Chem Commun 2004;2758.
[45] Yao YS, Xiao J, Wang XS, Deng ZB, Zhang BW. Adv Funct Mater 2006; 16:709.
[46] Wang LH, Kang ET, Huang W. Polymer 2001;42:3949.
[47] Burn PL, Grice AW, Tajbkhsh A, Bradley DDC, Thomas AC. Adv Mater 1997;9:1171.